Post-earthquake landslide distribution assessment using Sentinel-1 and -2 data: example of 2016 Mw 7,8 earthquake in New Zealand

Jan Jelének ¹,*, Veronika Kopačková ¹ and Kateřina Fárová ¹

¹ Czech Geological Survey; jan.jelenek@geology.cz
* Correspondence: jan.jelenek@geology.cz; Tel.: +420-257-531-376
Published: date
Academic Editor: name

Abstract: Post-earthquake analysis using radar interferometry has become a standard procedure for assessing earthquakes with significant damages. Sentinel-1 satellite provides 6-day revisiting time, Sentinel-2 data has 5-day revisiting time and the same viewing angle which can enable detecting changes in surface/land-cover after major seismic event. Using Sentinel-2 alongside with Sentinel-1 could bring new benefits when gathering spatial information of post seismic event. In our study we focused on analyzing major earthquake, which occurred on 14 November 2016 with 7,8 magnitude nearby the city of Kaikōura, New Zealand, using both Sentinel-1 radar images and Sentinel-2 optical data. Hundreds of landslides were reported as a result of this earthquake. In addition, substantial land uplift was detected in some parts of the sea shore. Differential interferometry allowed us to estimate earthquake strength analyzing the distribution of absolute vertical displacement values. Sentinel-2 pre- and post-earthquake images were used in order to assess land-cover changes and automatically detect landslides, which occurred after the earthquake. Linking DInSAR results with Sentinel-2 change detection analysis helped us to get a more complex perspective on the earthquake impact, to create landslide inventory maps and subsequently develop workflows for quick post-event analysis.

Keywords: Kaikōura earthquake; landslide detection; DInSAR; Sentinel-1; Sentinel-2

1. Introduction

Earthquake impact assessment and subsequent landslide mapping have become one of the crucial tasks which follow after a seismic event occurs. A strong earthquake can potentially trigger thousands of landslides. Usually, the spatial extent which is affected by a strong earthquake could be very big. In case of Kaikōura earthquake up to hundreds square kilometers were affected, which made it hard to quickly assess landslides using traditional mapping techniques. Radar interferometry offers substantial operational advantages over optical sensors, such as weather independence. Since introduction of the ESA´s Sentinel-1B satellite, radar data has been made freely available at 6-day revisit time. Radar data has been already successfully used to assess earthquake triggered landslides [1], although usually using L-band radar data (e.g., ALOS-PALSAR, JAXA) were used. When sensing surface changes, L-band radar data has an advantage over C-band, as it penetrates through vegetation and thus can get better coherence values.

Earthquakes usually cause vertical changes and displacements in affected areas as one of the major effects. One of the prominent techniques that can quantify such changes is satellite-based differential synthetic aperture radar interferometry (DInSAR) technology. This technique enables to detect and measure displacements of the Earth´s surface over the period of time. DInSAR exploits the

43 information contained in the radar phase before and after the earthquake takes place. It includes
44 interferogram formation and the phase difference calculation between two satellite acquisitions taken
45 from almost the same satellite position [2]. The phase difference can have multiple contributions
46 from: a flat Earth phase, topography, atmospheric effects, a phase noise and a possible ground
47 displacement component in the line-of-sight (LOS) direction [3]. The sensitivity of the DInSAR
48 technique for displacements is usually in millimeters and can be used for long-term monitoring of
49 landslides [4]. Besides identification of slow vertical motions, differential interferometry can be
50 potentially used for detecting surface changes, which occur after strong earthquakes.

51 Sentinel-2 has been used in studies regarding detection of temporal changes in the crops [5-7],
52 although when focusing on post-earthquake assessment, it has a limitation regarding the weather
53 and cloud coverage. With Sentinel-2B operational satellite, the revisiting time was reduced to 5 days,
54 which makes Sentinel-2 much more applicable. Combining SAR data with optical data thus can bring
55 a great benefit in evaluation of catastrophic events. There have been some studies, which focused on
56 combining SAR data with optical data, but none of them focused directly on earthquake impacts
57 assessment. Combination of SAR data and Landsat data was successfully used for agriculture studies
58 [8], forest structure mapping [9] and also recently in landslide mapping in Kenya [10]. To our best
59 knowledge, there is no study combining Sentinel-1 and Sentinel-2 data for seismic and post-seismic
60 hazard assessment, while mostly working with above mentioned Landsat data or simulated Sentinel-
61 2 data [7]. Sentinel-2 in comparison with Landsat-8 offers higher spatial resolution for selected bands
62 (10 m in visible to near infrared bands) which allows mapping landscape changes at a higher spatial
63 deatail.

64 The 2016 Mw7.8 Kaikōura earthquake occurred in the northeastern region of the South Island,
65 New Zealand on November 13th 11:02 (UTM). The damaging earthquake generated extreme surface
66 displacements, land deformations and surface ground motions [11]. Detailed description of M7.8
67 Kaikōura complex rupture process is given by [12]. Hundreds of landslides were reported as a
68 consequence of the earthquake. Most of the landslides were located in Hurunui District, North
69 Canterbury, around Cape Campbell in Marlborough and in Kaikōura Ranges [12].

70 In our paper, we demonstrate how DInSAR results derived from Sentinel-1 data and Sentinel-
71 2 change detection analysis can be used to develop workflows for quick post-event analysis, to create
72 landslide inventory maps, and overall, to get a complex perspective on the earthquake impacts.

73 **2. Experiments**

74 *2.1 Satellite data*

75 Tables 1 and 2 summarize used satellite data.

76

Table 1. Overview of Sentinel-1 scenes used

	Date	Perpendicular baseline	Temporal baseline	Track	Pass
Sentinel-1A south	3. 11. 2016 - 15. 11. 2016	-9,84 m	12 days	52	ascending
Sentinel-1A north	3. 11. 2016 - 15. 11. 2016	-8,65 m	12 days	52	ascending

77

78

Table 2. Overview of Sentinel-2 scenes used

	Date	Track	Pass
Sentinel-2A	3. 10. 2016	129	descending
Sentinel-2A	22. 11. 2016	129	descending

79

80

81   *2.2 Methods*

82   As it was stated above, studies combining optical and radar remote sensing for landslide
83   detection are up to now still rather rare. Both types of satellite data can serve simultaneously as a
84   source of different kind of information. In our study, we have used radar interferometry for vertical
85   displacement generation. We generated differential interferogram, which was phase-filtered using
86   Goldstein phase filtering and multilooked using SNAP software. Phase unwrapping was done using
87   Snaphu software. Displacement was then calculated from the unwrapped interferogram. Both
88   differential interferogram and displacement in LOS direction were georeferenced using Range-
89   Doppler Terrain Correction and used as quantification of earthquake impact and as indicators of the
90   distribution of landslides [16].
91   Sentinel-2 data used in our study were in the first step atmospherically corrected using the flat
92   field calibration (e.g, [17]). Cirrus clouds and thick clouds, snow and water were mapped and masked
93   out from the Sentinel-2 reflectance data. In order to map newly triggered landslides, vegetation cover
94   was mapped in both images before and after the earthquake. To differentiate surfaces covered by
95   vegetation from exposed surfaces atmospherically resistant vegetation index (ARVI, [18]) was
96   calculated. Unlike NDVI, this index is much less susceptible to atmospheric effects and thus can
97   overcome some of the atmospheric-induced errors. Differences in mapped surface water classes were
98   also assessed as these could be caused by landslides or the earthquake itself. Both radar and optical
99   based layers were matched with fault network and with the database of historical landslides in New
100   Zealand, which is available to the public by the GNS Science (formerly Institute of Geological and
101   Nuclear Sciences Limited) (Lower Hutt, New Zealand).

102   **3. Results and discussion**

103   Landslides triggered by the Kaikōura earthquake occurred within very wide area characterized
104   by complex terrain. Changes in vegetation cover were mapped using two scenes of Sentinel-2 and
105   together with the vertical displacement obtained from an interferometric pair of Sentinel-1 images
106   served as a basis for landslide analysis triggered by the earthquake. Figure 1 shows two maps with
107   two results of differential interferometry. Differential interferogram (A) was clipped by relevant
108   coherence (> 0.5). Together with the displacement in the direction of LOS it is possible to identify the
109   most affected area. The maximum displacement was around 1,5 meter in the inland part with
110   significant displacement continuing towards the sea shore (B).
111   Landslides were mapped from the Sentinel-2 images over the most affected area of the South
112   Island, see vertical displacement map (Fig. 1 - B). Mapped landslides were displayed together with
113   the vertical displacement from the Sentinel-1 data and faults based on [19] (Fig. 2). Areas,
114   representing clusters of landslides mapped by [20] within first three months after the earthquake
115   (hashed polygons, Fig. 2), cover only some parts of the affected area. Results showed that all major
116   landslides mapped by [20] for some affected areas corresponded very well with the landslides
117   detected on the basis of Sentinel-2 images (Fig. 3). However, using Sentinel-2 data we were able to
118   map potential landslides within the whole affected area. We can conclude, that most of the landslides
119   identified from Sentinel-2 data are spatially connected with the known fault systems and within the
120   areas characterized by higher vertical displacement values (>700 mm).
121   In addition to landslides, new lakes/water bodies, created when new landslides
122   blocked/changed the water/river flows, can be potentially dangerous. In our study, Sentinel-2 data
123   allowed mapping such new water bodies, which is demonstrated in Figure 3 on example of the big
124   water body resulting from the Hapuku landslide, the biggest landslide triggered by the Kaikōura
125   earthquake with total area reaching 2 km^2.

126
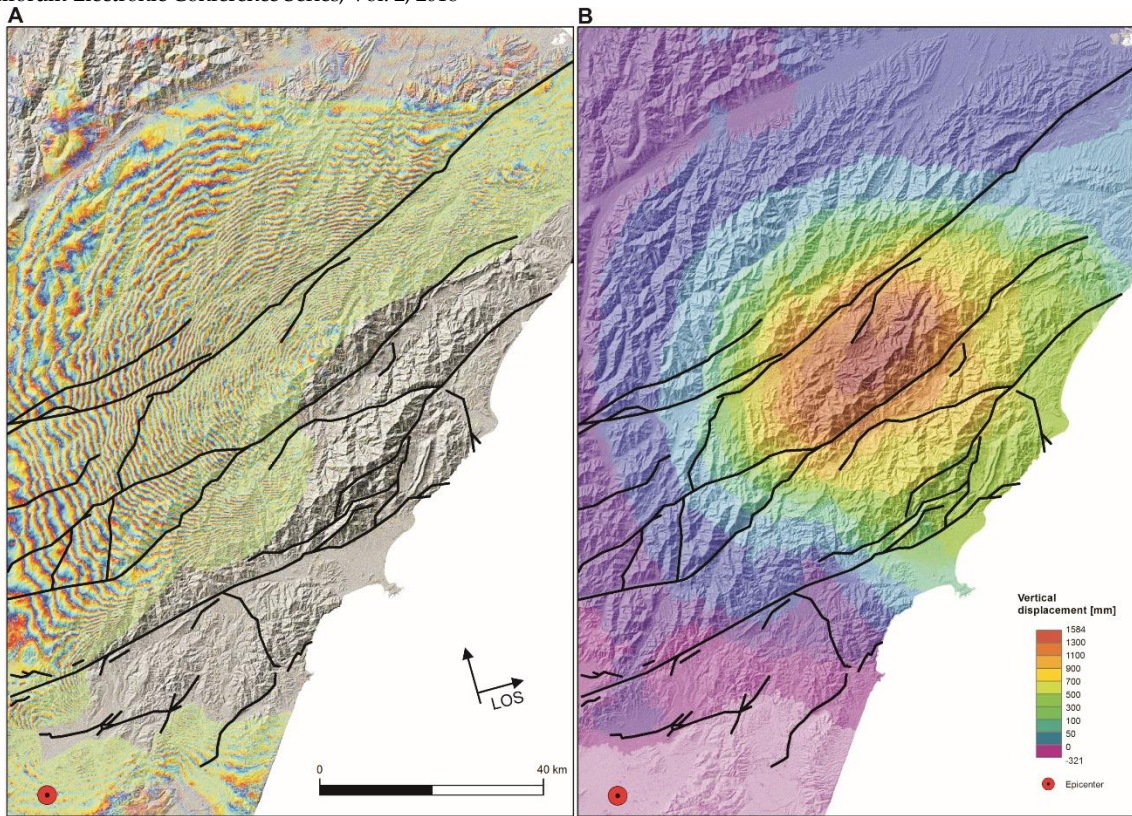
Figure 1. Two maps showing differential interferogram from Sentinel-1 data acquired between 3.11.2016 and 15.11.2016 (**A**) and displacement in LOS direction generated from the same interferometric pair (**B**) are overlaid by major faults and the Kaikōura earthquake epicenter.
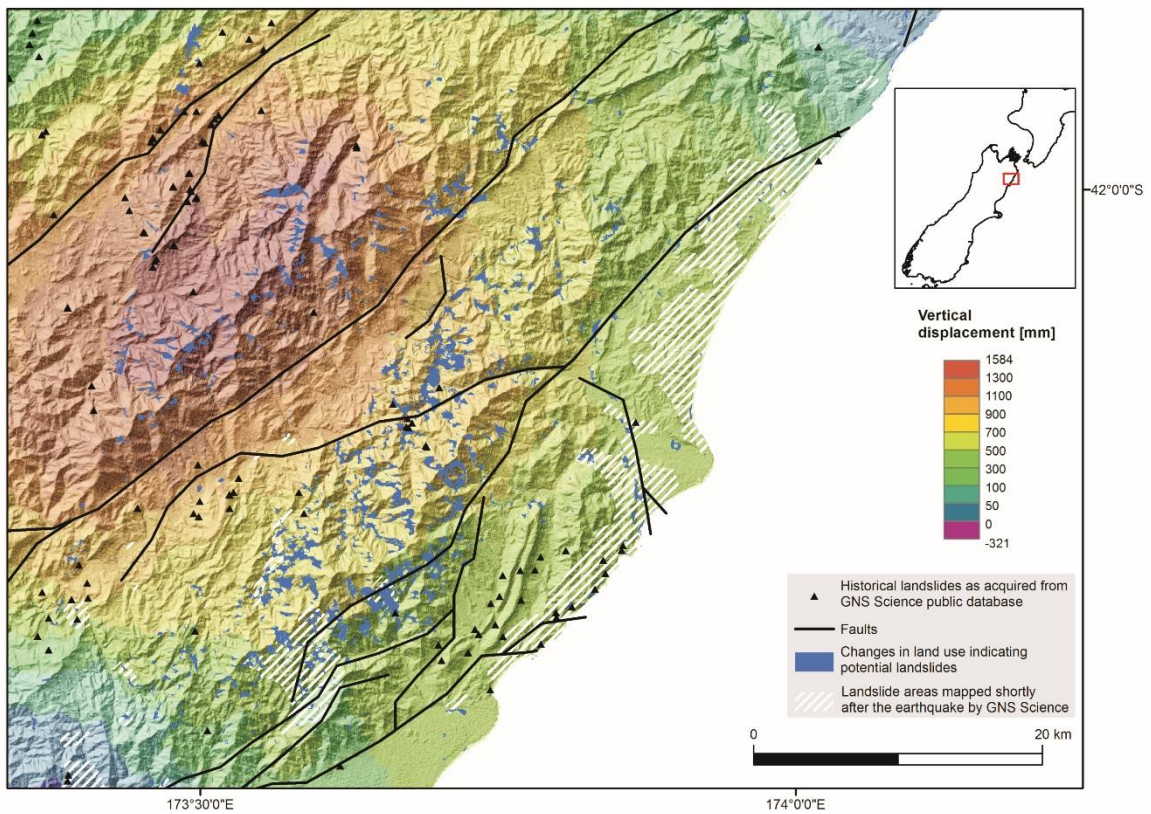
133 **Figure 2.** Map shows areas which changed its surface to bare soil/rock following the Kaikōura
134 earthquake and which are likely to be landslides triggered by the earthquake (the blue polygons).

135
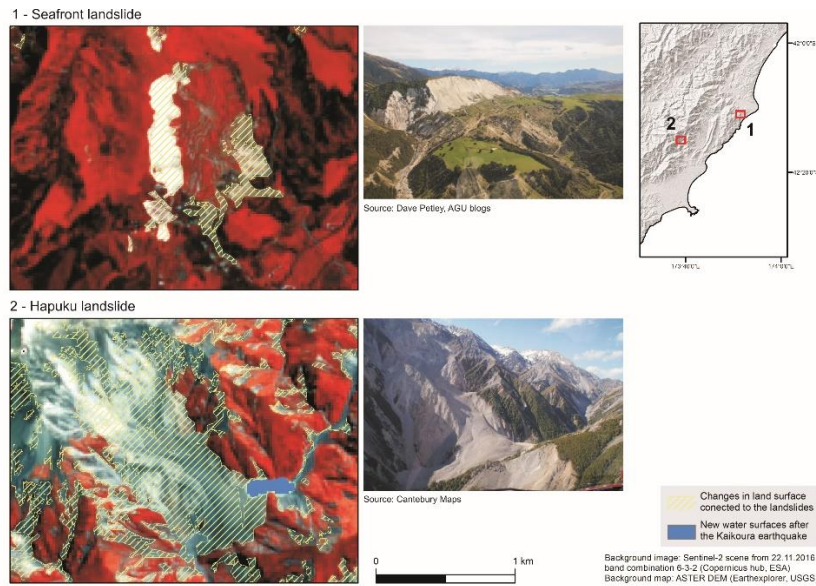
136

137 **Figure 3.** Two major landslides, caused by the Kaikōura earthquake derived from Sentinel-2 data.

138 **4. Conclusions**

139 Synergic use of Sentinel-1 interferometric products and products derived from Sentinel-2 optical
140 data could together allow quick assessment and complex earthquake impact analysis. Radar
141 interferometry allowed us to assess earthquake impacts via computing vertical displacements and
142 differential interferograms. Employing vegetation/water change detection on a basis of pre and post-
143 event Sentinel-2 data allowed us to identify the new landslides and water bodies resulting from the
144 Kaikōura earthquake. Sentinel-2 data provides more bands over visible (VIS) and near-infrared (NIR)
145 regions of the electromagnetic spectrum at a higher spatial resolution (up to 10-m) in comparison
146 with other satellites (e.g., Landsat), thus enable more detailed detection of land cover changes. Due
147 to the short revisiting time of both Sentinel-1 and Sentinel-2 satellites, it is possible to analyze major
148 seismic events and post-seismic impacts shortly after event occurrence over large areas and identify
149 critical "hot-spots" faster.

151 **Author Contributions:** Jan Jelének performed the processing work of the radar data and prepared a draft version
152 of the manuscript. Veronika Kopačková performed processing of the optical data. Kateřina Fárová helped with
153 the processing of the radar data.

154 **Conflicts of Interest:** The authors declare no conflict of interest.

155 **Abbreviations**

156 The following abbreviations are used in this manuscript:
157 ARVI: Atmospherically resistant vegetation index
158 DInSAR: Differential synthetic aperture radar interferometry
159 ESA: European Space Agency
160 LOS: Line of Sight
161 NDVI: Normalized difference vegetation index
162 SAR: Synthetic Aperture Radar

References

1. Czuchlewski, K.R., Weissel, .K., Kim, Y. Polarimetric synthetic aperture radar study of the Tsaoling landslide generated by the 1999 Chi-Chi earthquake, Taiwan. *Journal of Geophysical research* **2003**, 108, F1, 1-11. DOI: 10.1029/2003JF000037.

2. Hanssen, R. F. *Radar interferometry: data interpretation and error analysi*s, 1st ed.; Springer: Netherlands, 2001. ISBN 978-0-7923-6945-5

3. Osmanoglu, B., Sunar, F., Wdowinski, S., Cabral-Cano, E. Time series analysis of InSAR data: Methods and trends. *ISPRS Journal of Photogrammetry and Remote Sensing* **2016**, 115, 90-102. DOI: 10.1016/j.isprsjprs.2015.10.003.

4. Lazecký, M., Comut, F.C., Hlaváčová, I., Gürboga, S. Practical Application of Satellite-Based SAR Interferometry for the Detection of Landslide Activity. *Procedia Earth and Planetary Science* **2015**, 15, 613–618. DOI: 10.1016/j.proeps.2015.08.113.

5. Belgiu, M., Csillik, O. Sentinel-2 cropland mapping using pixel-based and object-based timeweighted dynamic time warping analysis. *Remote Sensing of Environment* 204, 509-523. DOI: 10.1016/j.rse.2017.10.005.

6. Valero, S., Mroin, D., Inglada, J., Sepulcre, G., Arias, M., Hagolle, O., Dedieu, G., Bontemps, S., Defourny, P. Processing Sentinel-2 image time series for developing a real-time cropland mask. 2015 IEEE International Geoscience and Remote Sensing Symposium (IGARSS), Milan, Italy, 26-31 July 2015, IEEE. DOI: 10.1109/IGARSS.2015.7326378.

7. Veloso, A., Mermoz, S., Bouvet, A., Le Toan, T., Planells, M., Dejoux, J.-F., Ceschia, E. Understanding the temporal behavior of crops using Sentinel-1 and Sentinel-2-like data for agricultural applications. *Remote Sensing of Environment* **2017**, 199, 415-426. DOI: 10.1016/j.rse.2017.07.015.

8. Amorós-López, J., Gómez-Chova, L., Alonso, L., Guanter, L., Zurita-Milla, R., Moreno, J., Camps-Valls, G. Multitemporal fusion of Landsat/TM and ENVISAT/MERIS for crop monitoring. *International Journal of Applied Earth Observation and Geoinformation* **2013**, 23, 132-141. DOI: 10.1016/j.jag.2012.12.004.

9. Hyde, P., Dubayah, R., Walker, W., Blair, J.B, Hofton, M., Hunsaker, C. Mapping forest structure for wildlife habitat analysis using multi.sensor (LiDAR, SAR/InSAR, ETM+, Quickbird) synergy. *Remote Sensing of Environment* **2006**, 102, 63-73. DOI: 10.1016/j.rse.2006.01.021.

10. Mwanki M.W., Kuria, D.N., Boitt, M.K., Ngigi, T.G. Image enhancements of Landsat 8 (OLI) and SAR data for preliminary landslide identification and mapping applied to the central region of Kenya. *Geomorphology* **2017**, 282, 162-175. DOI: 10.1016/j.geomorph.2017.01.015.

11. Wotherspoon, L.M., Palermo, A., Holden C. The 2016 Mw7.8 Kaikōura Earthquake: An Introduction. *Bulletin of the New Zealand Society for Earthquake Engineering* **2017**, 50, 2. ISSN: 11749857.

12. Duputel, Z. and Rivera, L. Long-period analysis of the 2016 Kaikōura earthquake. *Physics of the Earth and Planetary Interiors* **2017**, 265, 62-66. DOI : 10.1016/j.pepi.2017.02.004.

13. Castaldo, R., De Novellis, V., Solaro, G., Pepe, S., Tizzani, P., De Luca, C., Bonano, M., Manunta, M., Casu, F., Zinno, I., Lanari, R. Finite element modelling of the 2015 Gorkha earthquake through the joint exploitation of DInSAR measurements and geologic-structural information. *Tectonophysics* **2017**, 714-715, 125-132. DOI: 10.1016/j.tecto.2016.06.037

14. Matějíček, L. and Kopačková, V. Changes in Croplands as a Result of Large Scale Mining and the Associated Impact on Food Security Studied Using Time-Series Landsat Images. *Remote Sensing* **2010**, 2, 6, 1463-1480. DOI: 10.3390/rs2061463

15. Kaufman, Y.J. and Tanre, D. Atmospherically resistant vegetation index (ARVI) for EOS-MODIS. *IEEE Transactions on Geoscience and Remote Sensing* **1992**, 30, 2, 261-270. DOI: 10.1109/36.134076.

16. Langridge, R.M., Ries, W.F., Litchfield, N.J., Villamore, P., Van Dissen, R.J., Barell, D.J.A., Rattenbury, M.S., Heron, D.W., Haubrock, S., Townsend, D.B., Lee, J.M., Berryman, K.R., Nicol, A., Cox, S.C., Stirling, M.W. The New Zealand Active Faults Database. *New Zealand Journal of Geology and Geophysics* **2016**, 59, 1, 86-96. DOI: 10.1080/00288306.2015.1112818.

17. Rathje, E., Little, M. Wartman, J., Athanasopoulos-Zekkos, A., Massey, C. and Sitar, N. Preliminary Landslide Inventory for the 2016 Kaikoura, New Zealand Earthquake Derived from Satellite Imagery and Aerial/Field Reconnaissance. Version 1 (January 4, 2017). Quick Report 1, ver. 1 of the forthcoming NZ-US Geotechnical Extreme Events Reconnaissance (GEER) Association Report on the Geotechnical Effects of the 2016 M7.8 Kaikoura Earthquake.

215

218